

## Comparison of Titan's Equatorial Dunes to Lambertian Titan Surface Simulations\*

GABRIEL M STEWARD,<sup>1</sup> JASON W. BARNEs,<sup>1</sup> WILLIAM MILLER,<sup>1</sup> SHANNON MACKENZIE,<sup>2</sup> AND OTHERS?

<sup>1</sup>*University of Idaho, Moscow, Idaho 83844*

<sup>2</sup>*Johns Hopkins University Applied Physics Laboratory, Laurel, Maryland 20723*

### ABSTRACT

**NOTE: Red notes are important! Do not submit the document with any of them remaining!**

**NOTE: Blue notes are placeholders! Do not submit the document with any of them remaining!**

The nature of Titan's surface is poorly understood largely due to the atmosphere's extensive interference. We simulate lambertian Titan models using the radiative transfer program SRTC++ at different surface albedos. We then compare these models to real data from Cassini VIMS (Visual and Infrared Mapping Spectrometer) of the HLS (Huygens Landing Site) and equatorial dunes. We confirm that SRTC++ produces reasonable phase functions for lambertian surfaces shrouded by Titan's atmosphere in many, but not all, situations. Furthermore, we find that Titan's dunes act as lambertian surfaces, with all identified deviations correlating to suspected SRTC++ or atmospheric model deficiencies. This is in stark contrast to the other icy moons of the Saturnian system, which exhibit notable opposition effects.

**Keywords:** KEYWORDS (111) — KEYWORDS (112)

### 1. INTRODUCTION

Titan has one of the least understood surfaces in the entire Solar System, due largely to its thick haze-filled atmosphere that is opaque to most light. While there do exist a handful of atmospheric "windows" through which specific wavelengths of light can pass through relatively unimpeded (Barnes et al. 2007), only limited spectral information on the surface can be gleaned through them. Even within the windows, the thick atmosphere contaminates the relatively small amount of surface information we do receive; transmission is never perfect (Es-sayeh et al. 2023).

To combat this, we turn to radiative transfer models of Titan's atmosphere that predict the influence the atmosphere has on the received signal, allowing for true surface effects to be identified. Many such models have been created over the years, each with their own strengths and weaknesses (Griffith et al. (2012); Xu et al. (2013); Barnes et al. (2018); Corlies et al. (2021); Rannou et al. (2021); and Es-sayeh et al. (2023), to name a few). **Should we make sure to get ALL of these?** These radiative transfer models depend on accurate knowledge of Titan's atmosphere, which is most well characterized at the moon's equatorial regions since that is where the Huygens lander measured the atmosphere (Tomasko et al. 2008). Many surface characterization studies attempting to filter out the influence of the atmosphere have been performed in the

<sup>41</sup> past (Buratti et al. 2006; Soderblom et al. 2009; Kazeminejad et al. 2011; Brossier et al. 2018; Es-sayeh et al. 2023; Solomonidou et al. 2024). However, the majority of them <sup>44</sup> make a notable assumption: that the surface behaves as lambertian; a perfect scatterer with no directly reflected components. Buratti et al. (2006) is a notable exception.

<sup>47</sup> The lambertian assumption is considered reasonable for <sup>48</sup> the equatorial regions, as the highly reflective lakes and seas <sup>49</sup> of Titan are restricted to the poles (Hayes 2016). However, <sup>50</sup> other solid bodies in the Solar System exhibit non-lambertian <sup>51</sup> behaviors such as the prevalent opposition effect (Déau et al. <sup>52</sup> 2009). All this casts doubt on the lambertian assumption: <sup>53</sup> one would think Titan's surface would have non-lambertian <sup>54</sup> features as well, just ones that are obfuscated by the atmosphere, particularly since the other Saturnian moons exhibit <sup>55</sup> strong opposition effects (Kulyk 2008).

<sup>57</sup> In this paper, we seek to demonstrate the degree to which <sup>58</sup> Titan's equatorial dunes exhibit non-lambertian behavior. We <sup>59</sup> compare lambertian simulations of Titan with real observations of the dunes, identifying notable differences.

<sup>61</sup> The vast majority of observations of Titan's surface have <sup>62</sup> been done by spacecraft visiting Saturn, with the most high- <sup>63</sup> quality data coming from the Cassini mission. As such, many <sup>64</sup> images of Titan's surface are taken at unusual viewing geometries. This is quite useful, as it allows characterization of <sup>66</sup> Titan's surface from a wide variety of orientations, making it <sup>67</sup> far easier to determine exactly how non-lambertian a terrain <sup>68</sup> is. Unfortunately, most current radiative transfer models ap-

\* Sep, 22, 2025

69 pliable to Titan either assume a plane parallel atmosphere in  
70 their calculations (Griffith et al. 2012; Es-sayeh et al. 2023),  
71 don't consider angle at all (Rannou et al. 2021), or use a  
72 spherical approximation (Corlies et al. 2021). Thus, all these  
73 lose accuracy the further the viewing geometry is from direct  
74 illumination, and would miss potential non-lambertian ef-  
75 fects. To gain the useful information contained within obser-  
76 vations at non-ideal viewing geometries, the spherical nature  
77 of Titan's atmosphere must be considered. Thus, to create  
78 our lambertian models, we use SRTC++ (Spherical Radiative  
79 Transfer in C++), a radiative transfer code tailored to model  
80 Titan in full spherical geometry at the infrared wavelengths  
81 available to Cassini's VIMS (Visual and Infrared Mapping  
82 Spectrometer) instrument (Barnes et al. 2018). Other spheri-  
83 cal models do exist (Xu et al. 2013), but SRTC++ was chosen  
84 due to familiarity with the code.

85 Equipped with a spherical radiative transfer model and at-  
86 mospheric characterization from Huygens, it is now possible  
87 to compare models with reality on a scale covering the entire  
88 Cassini mission. As the equatorial regions are the best char-  
89 acterized atmospherically, we chose to examine the terrain  
90 there. While we examined multiple terrain types, it was de-  
91 termined that only the equatorial dunes had a sufficient num-  
92 ber of reliable observations to draw meaningful conclusions  
93 from. We also hand-picked observations from the Huygens  
94 Landing Site (HLS) for the sake of comparison, even though  
95 that location was only viewed at a limited number of view-  
96 ing angles. For both the dunes and HLS we compiled VIMS  
97 observations from across the entire Cassini mission over all  
98 available viewing geometries, limiting observations to only  
99 those judged to be of sufficient quality.

100 This analysis serves dual purposes—to qualitatively validate  
101 the SRTC++ simulation against real data, and to identify de-  
102 viations from lambertian behavior on Titan's surface. To ac-  
103 complish this, first we outline improvements made to SRTC++  
104 in **Model Methods** and report on those changes in **Model**  
105 **Results**. We describe the procedure by which we gathered  
106 our Titan data in **Observations and Data**, compare reality to  
107 simulation in **Model vs Data Comparison**, and end with the  
108 **Summary and Conclusion**.

109 **NOTE:** Be sure to redo this last introduction paragraph  
110 when the paper is done to match the final outline.

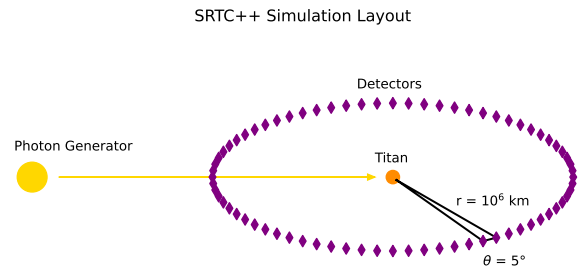
## 111 2. MODEL METHODS

112 **METHODS: Jason's Section.** Brief summary of  
113 SRTC++, citing the previous paper for more details. De-  
114 scribe new SRTC++ modules used, notably Absorption  
115 and the switch to Dose atmosphere. There should be  
116 a comparison figure to note the differences between the  
117 two. Mention the new integration method.

118 **Figs:** comparison between SRTC++ versions.  
119 Will be done by Jason

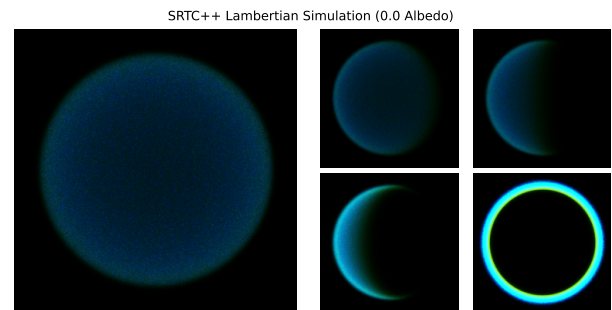
## 120 3. MODEL RESULTS

121 Four our work, we used SRTC++ to create three differ-  
122 ent models of a uniformly lambertian Titan, each run with  
123 a different surface albedo: 0.0, 0.1, and 0.2. Besides the  
124 albedo, the simulations were set up with identical parameters,  
125 as shown in **Figure 1**. The virtual detectors were set 10,000  
126 km away from the lambertian Titan, separated by 5 degrees  
127 and completely encircling the moon. Output was generated  
128 at all eight VIMS IR wavelength windows for Titan's atmo-  
129 sphere: 0.93, 1.08, 1.27, 1.59, 2.01, 2.69, 2.79, and 5.00  $\mu\text{m}$ .



130 **Figure 1.** Layout of our SRTC++ simulations. Distances not to  
131 scale. Detectors all equidistant from Titan and angular separation is  
132 the same for each one. The yellow arrow represents "photon pack-  
133 ets" being shot at Titan. Note that it does not interact with the de-  
134 tector it passes through.

135 **Figures 2-4** show the results of the simulations at 0.0, 0.1,  
136 and 0.2 albedo respectively, colored with 5.00  $\mu\text{m}$  as red,  
137 2.01  $\mu\text{m}$  as green, and 1.27  $\mu\text{m}$  as blue, as done in Barnes  
138 et al. (2005). The results of 0.1 are closest to the "green-  
139 ish" pictures of Titan in Barnes et al. (2005), though naturally  
140 without any terrain variation.



141 **Figure 2. NOT FINAL** Simulation results for a lambertian Titan  
142 with 0.0 albedo, colored with 5, 2 and 1.3  $\mu\text{m}$  mapped to red, green,  
143 and blue respectively. Left image is viewed at 0° from the incidence  
144 angle. Right four images are at 35°, 90°, 120°, and 180° in left  
145 to right then top to bottom order. [An animating version of the  
146 figure will exist in places that support it. The large left panel will  
147 hold the animating image, the right panels will remain static for  
148 comparisons]

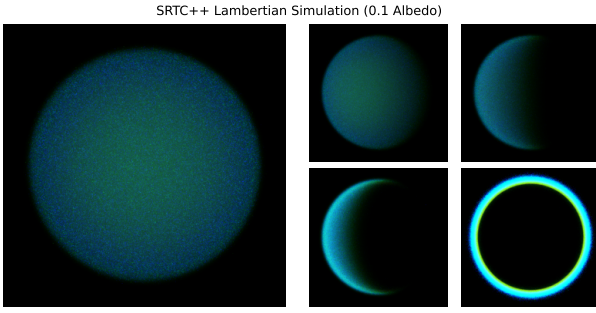


**Figure 3. NOT FINAL** Same as Figure 2 but for 0.1 Albedo.

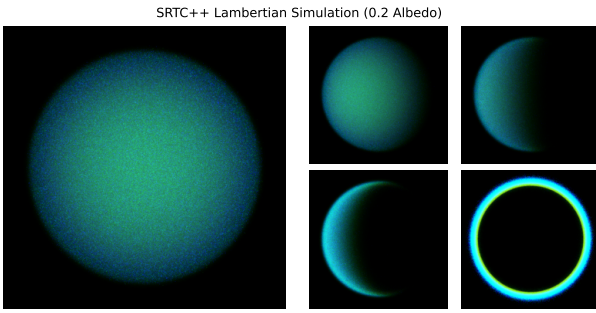


**Figure 4. NOT FINAL** Same as Figure 2 but for 0.2 Albedo.

The simulations are largely as expected for a lambertian sphere obscured by a thick atmosphere. We can see what a lambertian sphere should be without an atmosphere from Fig 9 in Pont & Koenderink (2007), and the 0.0 albedo simulation shows us the effect of the atmosphere without any signal coming from the surface. Both effects should be active in the 0.1 and 0.2 albedo simulations, and that is in fact what we see in the directly illuminated view: a greenish center where there's minimal atmospheric influence that slowly fades off as the observation angle becomes steeper, at which point the atmosphere takes over with its bluish hue. Note that the coloration is entirely due to atmospheric effects; bluer light is scattered in the atmosphere more readily than redder light. In the raw data the blue channel is the largest even in the center at 0.1 albedo, it is merely the choice of color balancing that gives Titan its greenish hue; a sensible choice as it allows us readily identify places with more surface signal than atmospheric. The center of the disc, when viewed from head on, is rather uniform with little variation, as it should be.

Views other than direct illumination also behave as expected; the edges are always atmospherically dominated, becoming bluer. Light is more likely to be forward scattered than backscattered in Titan's atmosphere (García Muñoz et al. 2017; Cooper et al. 2025), so the closer the Sun gets to behind Titan, the brighter the edges become. A lambertian surface without an atmosphere would have no light coming from anywhere that was not directly illuminated, but we see a small amount of light released from beyond the terminator

due to atmospheric scattering. We can also see the shadow Titan casts on its own atmosphere in the profile views as the signal gets abruptly diminished near the top and bottom of the moon, but the atmosphere above this shadow remains illuminated. This effect is known to happen on Earth as well and is what results in the colors of twilight (Lynch & Livingston 2004).

Notably the “eclipse” view at 180 degrees is functionally identical in all simulations, which it should be as the surface has little to no influence on the signal at this viewing geometry. There is most certainly interesting science to be done with the simulation at this angle to probe the atmosphere, but that is beyond the scope of this paper.

The simulation results notably appear slightly grainy. This is due to the Monte-Carlo nature of SRTCP++. If we were to run the simulation for longer, the S/N (signal to noise) would increase and the overall image result would become smoother. However, given as we end up averaging numerous pixels together for this work, such effort would be wasted.

We ultimately seek to compare these simulations with real data. And while we can qualitatively see that real Titan images do have similar coloration and limb effects (Barnes et al. 2005), the fact that real Titan has numerous different terrain types interferes with any more robust conclusions. As such, we turn these visual models into phase function models. These phase function models can, given a specific viewing geometry, predict how a lambertian Titan would appear at that geometry, which can then be compared to real data.

To construct the phase function models, every model pixel is sorted into bins based on viewing geometry and then their values are averaged. The bins are separated by 5 degree increments in incidence, emission, and azimuth angle, defined as shown in Figure 5, with  $0^\circ$  azimuth being the forward scattering direction, and  $180^\circ$  being the backscattering. We use these angles instead of the more standard bidirectional reflectance distribution function (BRDF) as that uses four variables to describe the situation, while our models only need three. With 3 different albedos and 8 wavelengths, we produce a total of 24 phase function models ready to be compared with similar phase functions compiled from real VIMS data.

#### 4. OBSERVATIONS AND DATA

Cassini performed over a hundred separate flybys of Titan during its mission (Seal & Bittner 2017), and most of those flybys have observations from Cassini VIMS. Viewing geometries on any single flyby are generally limited in scope, as the spacecraft itself could only examine geometries it personally encountered. Thus, in order to gain a proper understanding of the surface of Titan at a wide range of viewing geometries, observations from as many flybys as possible should be used.

Viewing Geometry Model: Incidence 40 Emission 23 Azimuth 34

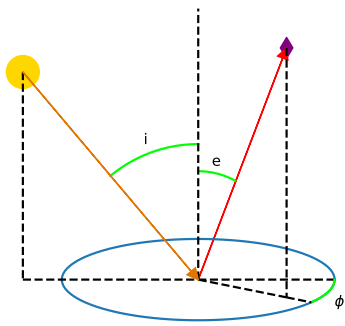


**Figure 5.** Viewing Geometry Angles used in this paper. Incidence angle is represented by “*i*”, emission angle by “*e*”, and azimuth angle by “ $\phi$ .” The arrows trace out a path from the sun (yellow circle), to some arbitrary spot on Titan’s surface, to a detector (purple diamond).

The primary obstacle in properly using all the data is the sheer amount in play; over a hundred flybys, tens of thousands of individual observations, and in each of those hundreds of spectels each with hundreds more individual values associated with them. If we wished to make a single global model, this would not be an issue, as an algorithm could easily ingest everything. However, simple inspection of VIMS images reveals different terrains have different albedos and our simulations above clearly show how much the appearance of the surface changes with albedo. Averaging all terrain types together could smooth out non-lambertian behavior, or allow a single non-lambertian terrain type to contaminate all the others.

As such, we need to limit our data to single terrain types. We also chose to focus on the equatorial regions between  $30^\circ$  and  $-30^\circ$  latitude since that’s where Huygens sampled the atmosphere (Tomasko et al. 2008), making this region the best characterized. We also want terrain types that are viewed from a wide variety of viewing geometries with a large number of reliable observations. We judged that only Titan’s dunes met all these criteria. (The equatorial bright terrain was considered as well, but the results we obtained from it were inconsistent and unreliable. See the [appendix](#) for more information.) In pursuit of this goal, we created a raster mask of Titan’s equatorial dunes (**Figure 6**).

The creation of the mask began with the Titan terrain map created by Lopes et al. (2020) using radar data. VIMS observations, which are taken in infrared, often don’t match the radar observations (Soderblom et al. 2007), but tend to agree in the bulk of major features; most notably (and importantly for this paper) the dunes have good agreement on a global scale.

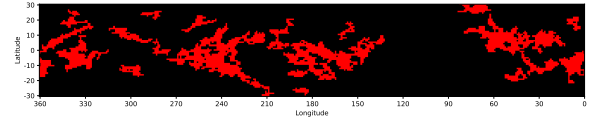


**Figure 6.** Titan equatorial surface terrain mask for dunes, as informed by Lopes et al. (2020) mixed with VIMS observations. Black areas are “Null” pixels as outlined in the text, while the red are dunes. Almost all of the dunes on Titan are included in this mask, though there are a few regions outside the  $30^\circ$  and  $-30^\circ$  latitude boundaries.

The resolution in question for the mask is one pixel per degree on Titan’s surface; 181 in latitude and 360 in longitude. The radar map was scaled down to reduce it to this resolution. Any pixel that was not clearly or nearly a solid color was replaced with a “Null” pixel; one where we would not harvest data from when using the mask to identify terrain. We erred on the side of caution, more likely to assign “Null” to a pixel than not. Any pixels of different terrains that were touching were marked “Null” as well to avoid contamination. After this we manually removed some areas that notably did not match VIMS data, were too small to be of use, or were known to have different spectral characteristics than other terrains given the same classification. Hotei Regio, Tui Regio, and Southern Xanadu were notable manual exclusions. The original mask had many different terrain types, but we reduced all non-dune terrains to “Null” for this paper.

In addition to the terrain classification in **Figure 6** the mask also has a version with a hidden data point: each pixel records its distance to the nearest “Null” pixel in km along Titan’s surface. This allows the mask to be refined: pixels that are close to “Null” pixels can be excluded as likely to have contamination from pointing errors in the VIMS data, which are known to occur (Barnes et al. 2008).

VIMS observations come in the form of “cub” files. Our investigation procedure for these files begins with a basic database search; in our specific case, looking for any cubs that have spectels in the equatorial regions between  $30$  and  $-30$  latitude, and also have spectels of 25 km ground resolution or lower. The database we are using has already filtered out clearly erroneous files, as well as so called “noodle” images which are only a handful of spectels in diameter.

Once the cubs are identified, they are ingested and each individual spectel examined to see if it is satisfactory according to provided restrictions; namely, the latitude and ground resolution limitations. If a spectel passes the test, it is added to a list. This list can be made with or without referring to the mask. When the mask is used, only spectels marked as dunes are cataloged. The spectels are then judged based on their proximity to a “Null” pixel on the mask. Two options exist for this: setting a minimum distance from a “Null” pixel that will be accepted, or setting an allowed maximum ratio of ground resolution to “Null” pixel distance. For this work, we

had a minimum “Null” distance of 50 km and a maximum ratio of ground resolution to “Null” pixel distance of 1/4.

When the mask is not used, “Null” values can be accepted. This is helpful when wanting to look at areas in or near “Null” pixels, such as the Huygens Landing Site.

We then bin the list of spectels and create a phase function out of them in a process identical to that described in [Model Results](#). Unlike other investigations, we do not subtract off atmospheric contributions as our simulations are complete with atmospheric contributions. This saves us considerable processing difficulties.

There are a few limitaitons to the created phase functions. The primary limitation is that certain viewing angles, usually at the extreme ends of allowed values, do not exist since Cassini was never in those positions. Particularly high resolution cubes can reveal small details not visible in most views and thus are not reflected in the mask, such as a handful of observations that can see interdune areas ([Barnes et al. 2008](#)). These small details need not match the behavior of the terrain they are surrounded by, and could conceivably offset the final model. For larger data sets, such as the dunes, situations like this are likely to be overcome by the sheer number of data points available at lower resolution. There is also no check for interfering clouds at this time.

In addition to the dunes, we also made a phase function for the Huygens Landing Site, as our atmosphere models ultimately draw from observations made by the Huygens lander ([Tomasko et al. 2008](#)). We performed a database search similarly to how we made the other models, but we also went in manually, cleaning up any situations where Cassini reported the wrong latitude and longitude for the spectels, ensuring that the data was devoid of any contamination; something we only had to do since the Huygens Landing Site was such a small area on the boundary of multiple terrain types. Unfortunately, there were relatively few viewing angles of the HLS despite it being among the most observed locaitons on Titan, which is why examining the dunes as a whole was necessary. In order to counteract this lack of data for both the dunes and the HLS, we performed tetrahedral interpolation to fill in as many observation angles as possible, using the PyVista package ([Sullivan & Kaszynski 2019](#)).

## 5. MODEL VS DATA COMPARISON

### 5.1. *Huygens Landing Site*

We choose to examine the HLS first as its data are simpler, though it covers significantly fewer viewing geometries than the dunes. As three-dimensional data are hard to visualize, we opt to plot individual “skewers” of data at a time, fixing two of the three viewing geometry angles while allowing the third to vary. We do this for all phase functions, be they models or real data. We plot select skewers of the three models and HLS data in [Figures 7-9](#).

Ignoring the HLS for a moment, the phase function models showcase a distinct shifting of behavior across the various wavelengths. The shorter wavelengths have rougher lines, while the longer ones are smoother. This is due to the general trend of the atmosphere having higher optical depth at shorter wavelengths ([Es-sayeh et al. 2023](#)), allowing for more scattering events in more directions, which in turn mean more simulation time would be required to smooth out all those directions.

We see characteristic behavioral differences in phase function behavior at the different wavelengths in [Figure 7](#) and [Figure 8](#), with the general shape of emission skewers in particular changing drastically between 0.93 and 5.00  $\mu\text{m}$ . When skewering across incidence or emission, this is common; though when skewering across azimuth the general shape is usually similar in all wavelengths, including the skewer shown in [Figure 9](#). Keep in mind that across these three figures only a small amount of the total models are shown, behavior can change significantly when skewering at different locations, though the transitions are always relatively smooth. These particular skewers were chosen because they are the places with the best HLS data visualizations.

The HLS data are very well behaved for the most part, with data that interpolates smoothly and forms lines that correspond rather well to the models. In 1.27 and 2.01  $\mu\text{m}$  the data lines up almost perfectly with the 0.1 albedo prediction, while the others sit somewhere between 0.0 and 0.1. 1.08  $\mu\text{m}$  hugs the 0.0 albedo line, and of all the wavelengths it shows the largest variation, most notable in [Figure 7](#) here, but the variation is also visible in other views not shown. We are unsure why 1.08  $\mu\text{m}$  in particular does this; we expect 0.93 and 1.08 data to be variable due to the large atmospheric contributions, but not for them to be much different from each other. Perhaps this is a feature of the HLS itself?

Even considering 1.08  $\mu\text{m}$ ’s quirks, the HLS appears consistent with a lambertian surface in all the viewing geometries we have access to, which admittedly is not very many. We chose the best skewers we could for [Figures 7-9](#), and even the azimuth skewer only covers about a third of the available values. Nothing probes the higher incidence and emission angles, and the extremes are aren’t even approached. This tells us nothing about SRTC++’s reliability beyond angles that are already probed well by other radiative transfer models. Thus, we move to a much larger data set: the dunes.

### 5.2. *Equatorial Dunes*

Similarly to the HLS data, we plot a variety of select skewers for the dunes in [Figures 10-12](#). We plot more than three as the dunes data cover a far wider range of viewing geometries.

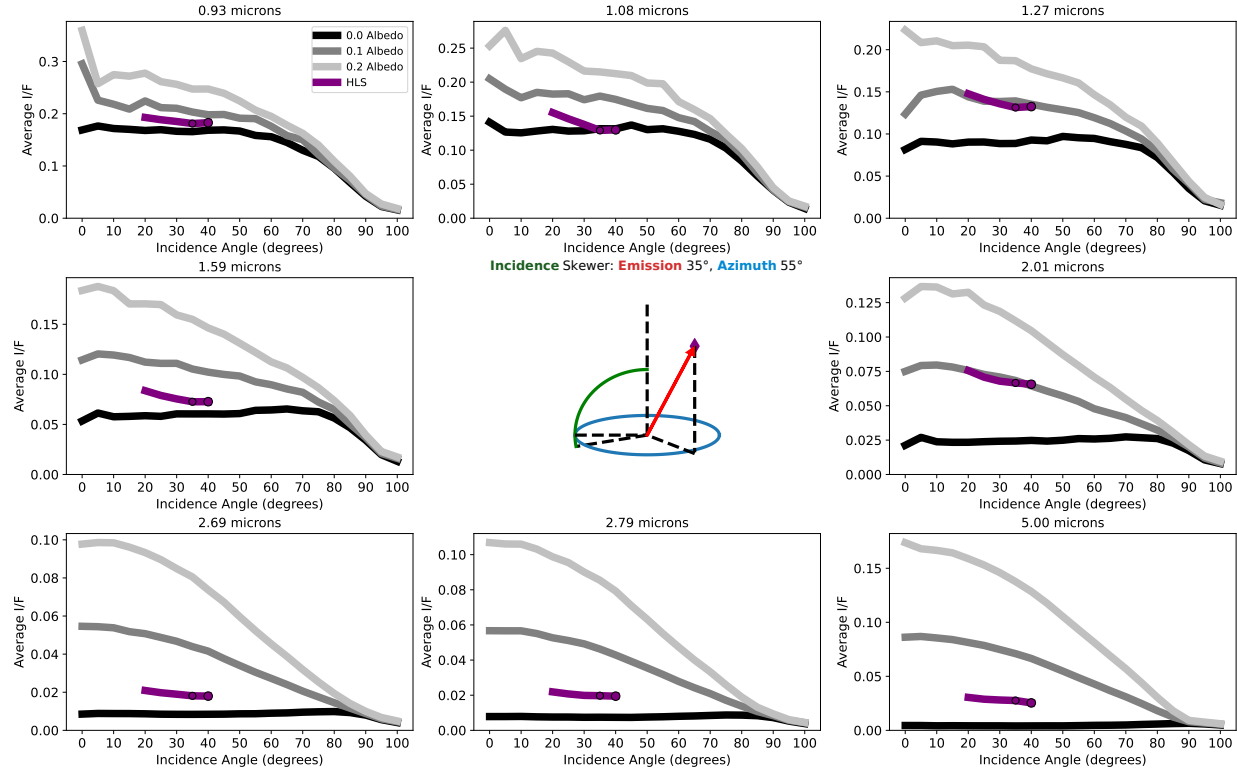


**Figure 7.** Incidence angle skewer: incidence angle versus average I/F comparing phase function models with HLS data with fixed emission and azimuth angles. Showcases all eight wavelengths arranged from shortest to longest, with the central area occupied by a geometry diagram to illustrate the exact situation plotted. Model lines are monochromatic, HLS data are purple. Places with direct HLS observations have dots plotted overtop of the lines, larger dots meaning more observations. Places on the HLS lines without dots are interpolated values. Note that the vertical axis scales with the data, not all wavelengths produce the same average I/F scale.

Beginning with incidence angle skewers, we find that most skewers share a similar shape, visible in both [Figure 10](#) and [Figure 11](#). Higher incidence angles have lower I/F across the board, the exception being skewers with high emission and low azimuth, but the dunes have no data at those viewing geometries so we ignore them. The dune data match the shape of the models very well in these views, though incidences higher than 80° should be taken with a grain of salt as there is very little data at those extreme angles, though the points that do exist behave as expected in these views.

Curiously, the 2 μm has a very noticeable shift in retrieved albedo for the dunes between [Figure 10](#) and [Figure 11](#), going from hugging the 0.1 albedo model to hanging somewhere around 0.05 albedo. 1.27 μm may do this as well, though it is harder to tell as the gap between 0.1 and 0.0 albedo models is smaller in that window and the data are less consistent. We will return to this effect when examining the emission skewers, as the effect is far more noticeable there.

Most incidence skewers not shown look like [Figure 10](#) and [Figure 11](#) in the phase function models, excepting those where there is no data. The dunes data usually match the models in shape rather well, indicating lambertian behavior when incidence is considered, with minor and momentary

deviations for the most part. However, there are exceptions, which happen at high emission and high azimuth, exemplified by [Figure 12](#). Here, the 2.01, 2.69, and 2.79 μm windows do not have slopes that match the models. Unfortunately, there isn't a very large spread of points at this view, so this anomaly is hard to draw things from. We will return to this, however, when examining the emission skewers.

[Figure 12](#) also makes clear a physical impossibility that sometimes crops up in incidence slices: while the 0.93 and 1.08 μm windows have dune phase function shapes that match the models', the retrieved albedo is below 0.0, an impossible. This may be because SRTC++ does not account for Rayleigh scattering, which is most relevant at short wavelengths ([Es-sayeh et al. 2023](#)). Intuitively, one would expect adding Rayleigh scattering to make the model brighter, not dimmer, but subtle effects could be at play—to fully answer this question we would have to implement Rayleigh scattering.

The emission skewers for the phase function models generally show gradual increases in brightness with larger emission, though 5 μm is a notable exception, along with low incidence and high azimuth views. Selected views can be seen in [Figures 13-15](#). [Figure 13](#) and [Figure 14](#) clearly show that

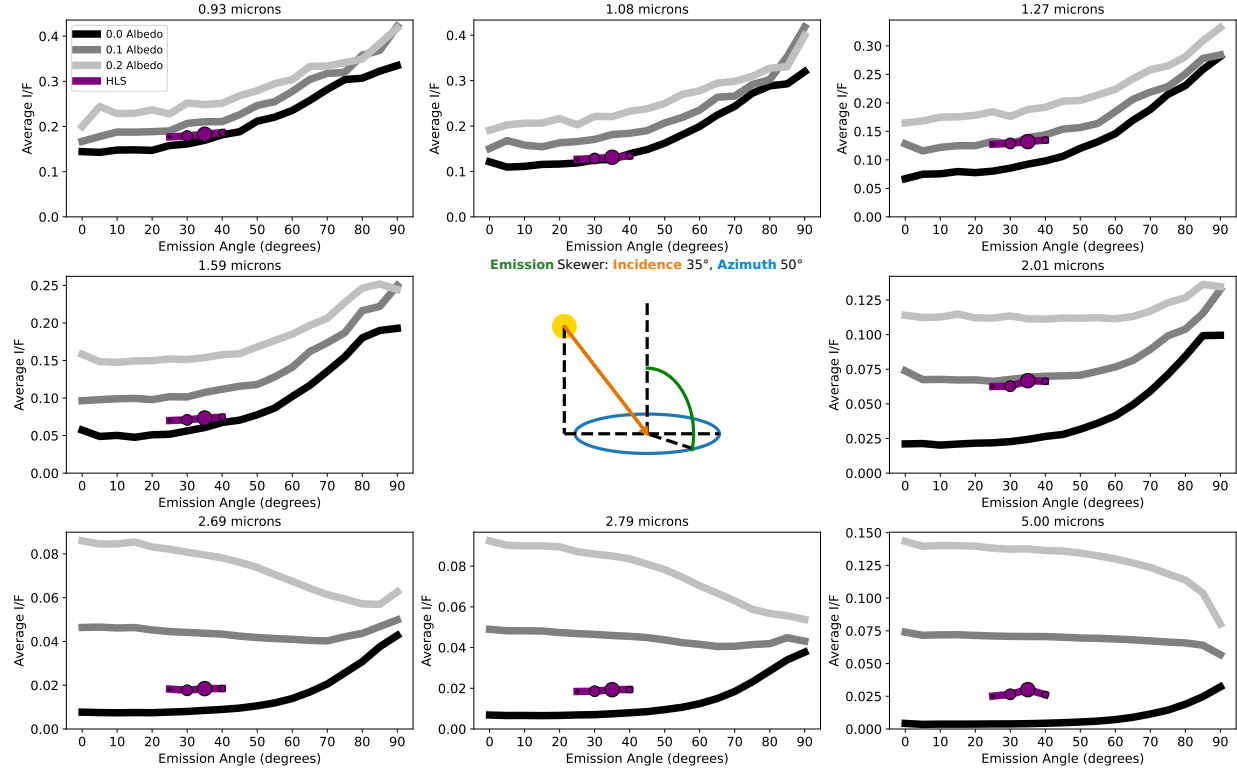


**Figure 8.** Same as [Figure 7](#) but is instead a skewer through the emission angle, with incidence and azimuth held fixed.

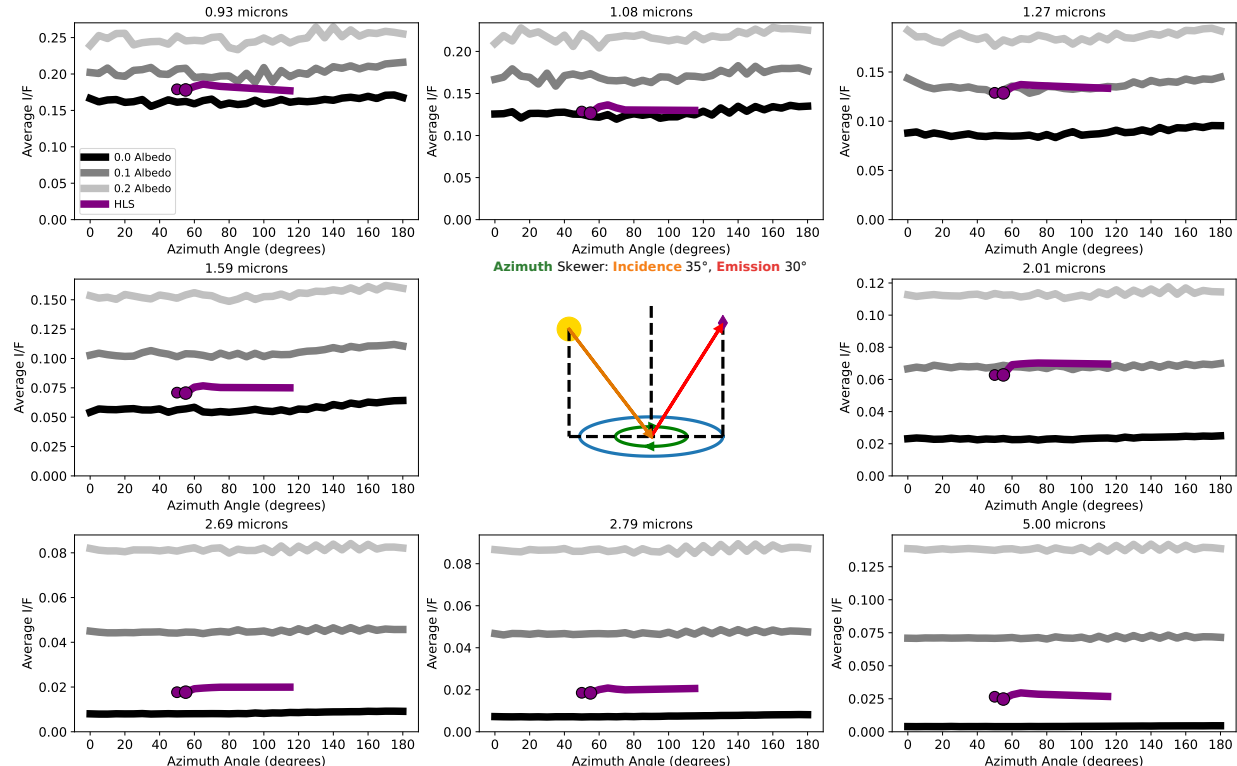


**Figure 9.** Same as [Figure 7](#) but is instead a skewer through the azimuth angle, with incidence and emission held fixed.

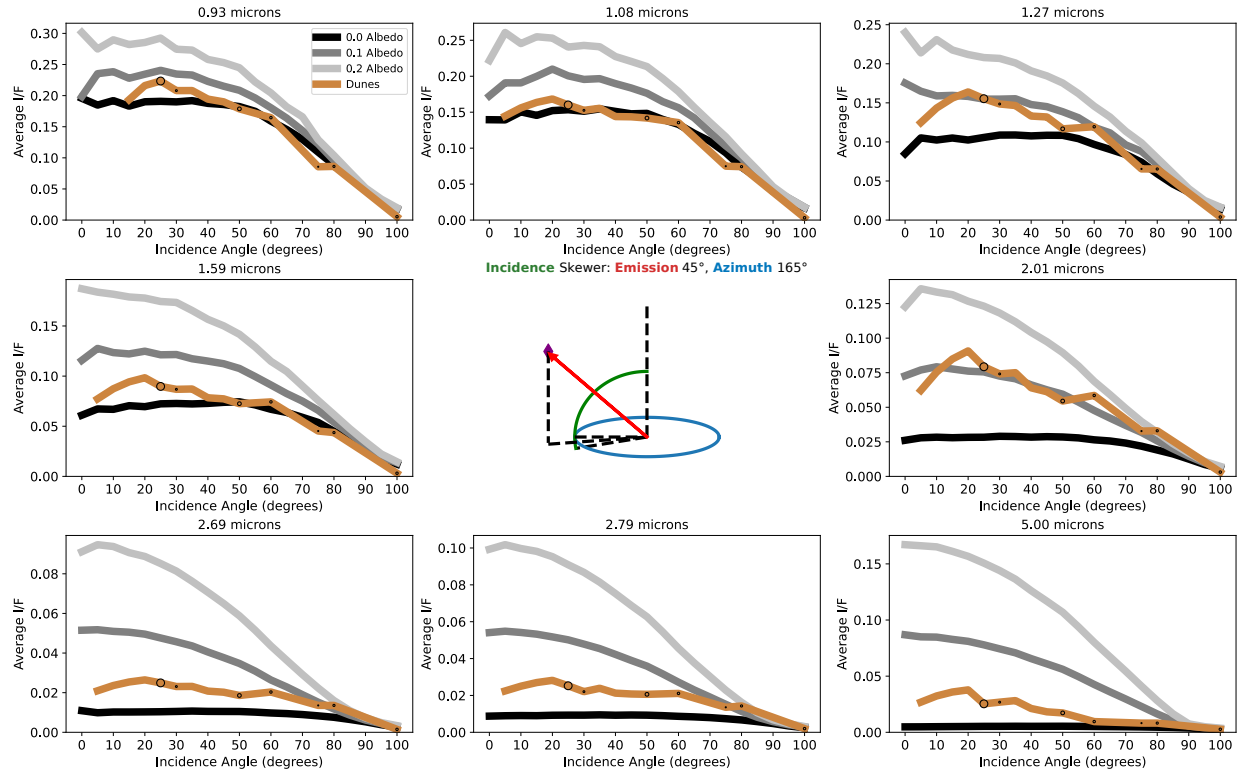


**Figure 10.** Incidence angle skewer: incidence angle versus average I/F comparing phase function models with dunes data with fixed emission and azimuth angles. Showcases all eight wavelengths arranged from shortest to longest, with the central area occupied by a geometry diagram to illustrate the exact situation plotted. Model lines are monochromatic, dunes data are brown. Places with direct dunes observations have dots plotted overtop of the lines, larger dots meaning more observations. Places on the dunes lines without dots are interpolated values. Note that the vertical axis scales with the data, not all wavelengths produce the same average I/F scale.

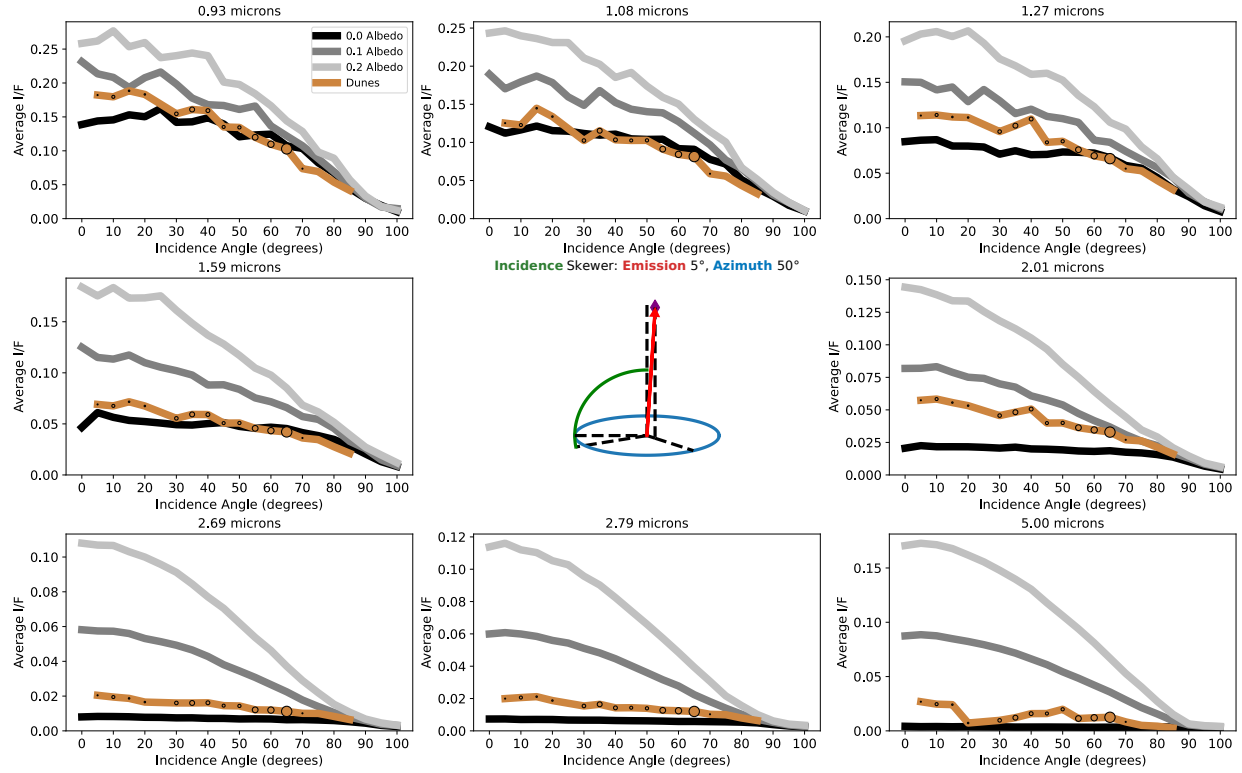


**Figure 11.** Same as [Figure 10](#) but at different fixed emission and azimuth angles.

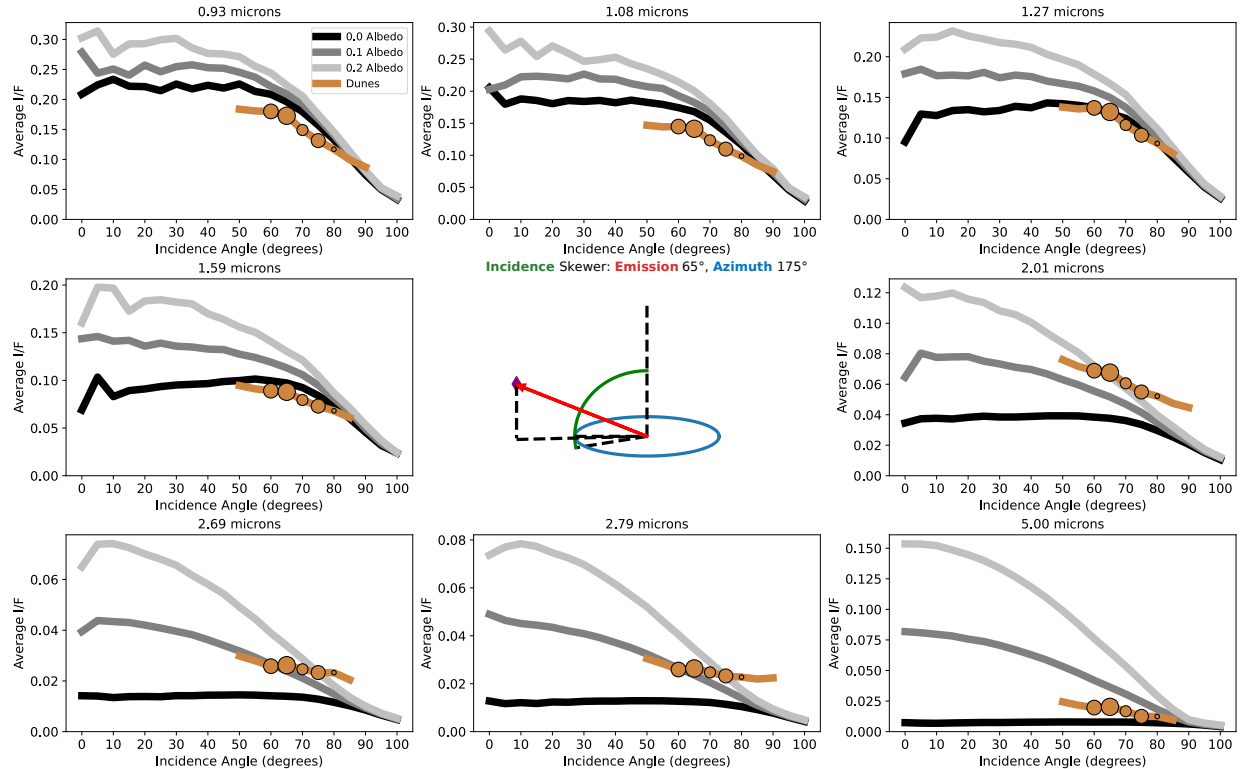


**Figure 12.** Same as [Figure 10](#) but at different fixed emission and azimuth angles.

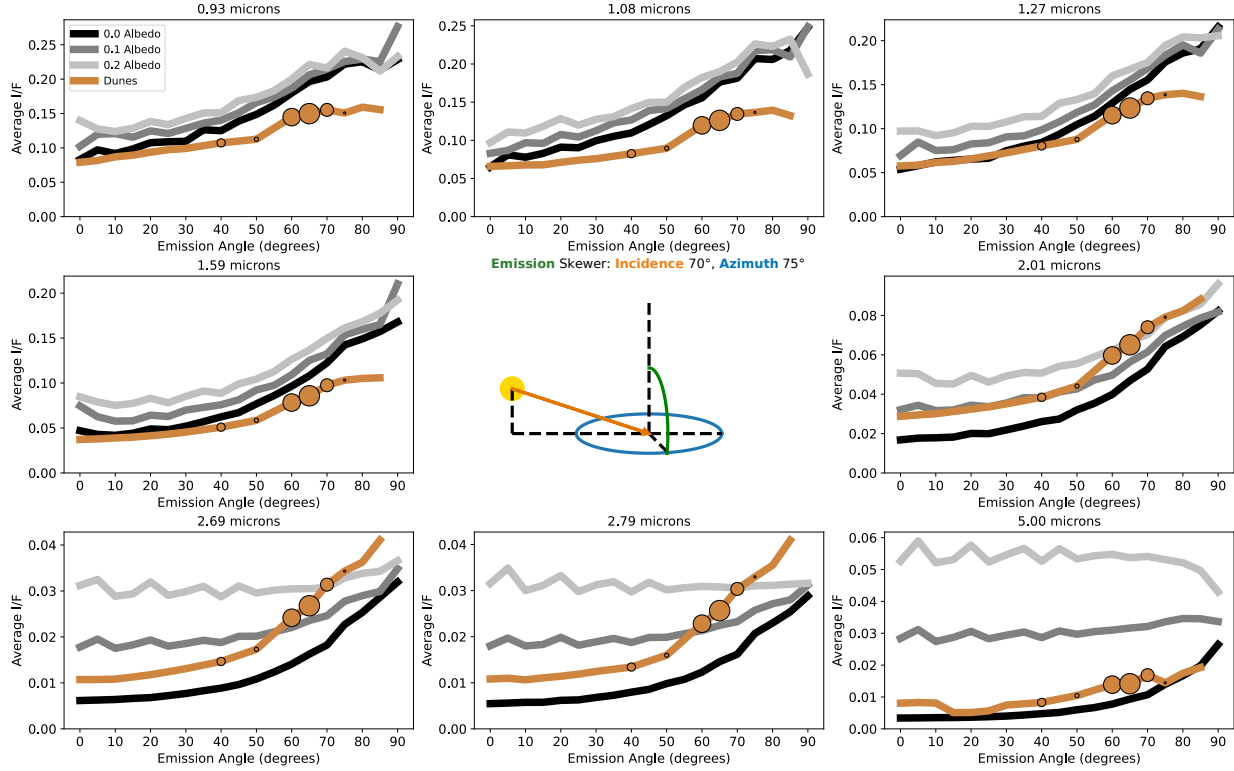


**Figure 13.** Same as [Figure 11](#) but is instead a skewer through the emission angle, with incidence and azimuth held fixed.

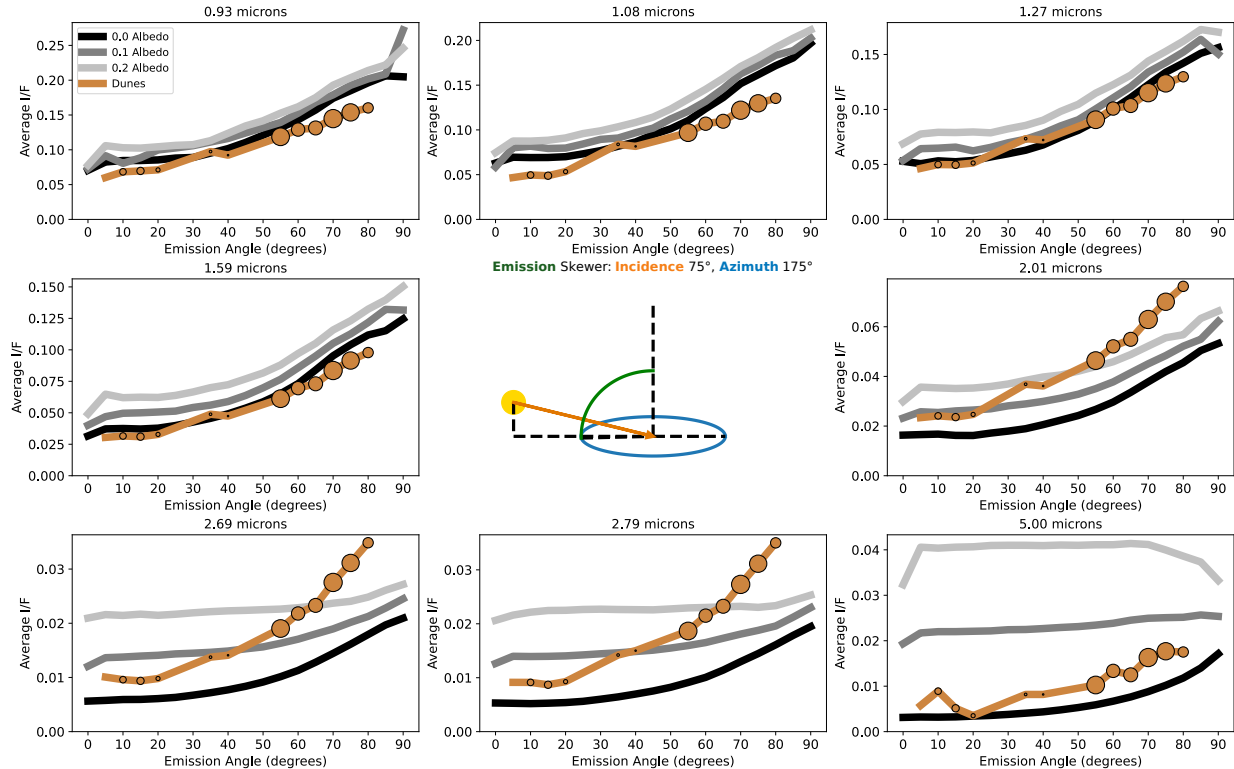


**Figure 14.** Same as [Figure 13](#) but at different fixed incidence and azimuth angles.

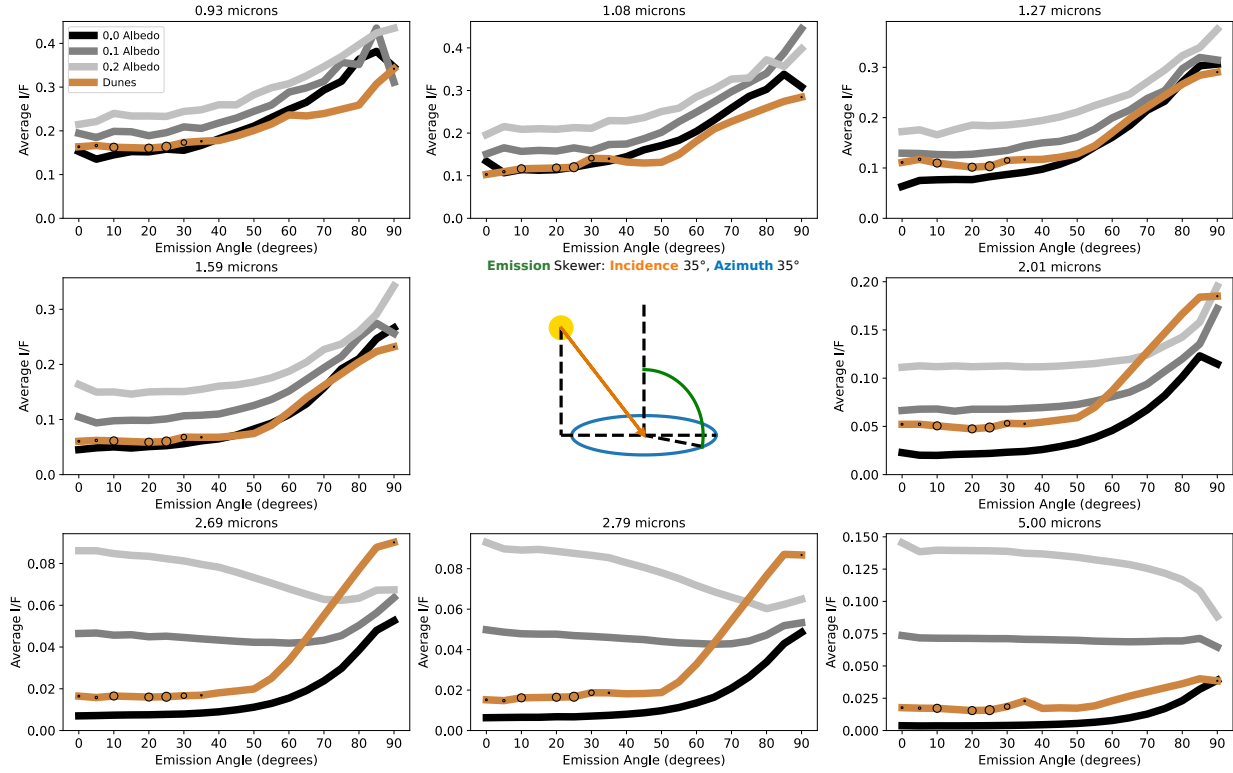


**Figure 15.** Same as [Figure 13](#) but at different fixed incidence and azimuth angles.

for low emission angles, up to around  $40^\circ$ , the data match the models pretty well. However, at higher emission angles, this fails: [Figure 13](#) shows the  $0.93 - 1.59 \mu\text{m}$  windows dipping below the 0.0 albedo model at higher emission, while  $2.01 - 2.79 \mu\text{m}$  do the opposite and sharply tick above the models. The dramatic brightening of  $2.01 - 2.79 \mu\text{m}$  is just as strong if not stronger in [Figure 14](#) showing azimuthal independence of this effect. However, the  $0.93 - 1.59 \mu\text{m}$  dimming below the 0.0 albedo model is not as strong, and doesn't clearly exist at the  $1.27 \mu\text{m}$  and  $1.59 \mu\text{m}$  windows. The dimming effect vanishes entirely in [Figure 15](#), while the brightening effect remains. (Notably, [Figure 15](#) has few data points at high emission, but the fact that it follows the pattern laid out in other skewers gives us confidence that its behavior is not just an interpolation artifact). These brightening and darkening effects at higher emission completely explain the inconsistent retrieved albedo and values below 0.0 albedo noted in the incidence skewers; these deviations are emission dependent. Furthermore, the fact that brightening only occurs in  $2.01 - 2.79 \mu\text{m}$  windows and these are the only windows seen not matching the models in [Figure 12](#) lends further credence that [Figure 12](#)'s deviations are not just a bad series of observations.

So, how can we explain these discrepancies? There are two primary explanations. First, the model is not accurately accounting for some atmospheric effect at high emission. **RE-SEARCH: what parts of the atmosphere could be influencing this? What papers would be relevant? This will take significant time to sort out.**

The second option is that we're seeing a true nonlambertian effect from the surface. However, this seems unlikely, as the brightening effect appears azimuthally agnostic: no matter what azimuth we point at, the effect exists where we have enough data to see it, and a forward-scattering or backscattering effect would be particularly focused at  $0^\circ$  or  $180^\circ$ , not present everywhere. Topography oriented explanations also seem unlikely, since the effect begins around  $40^\circ$  and only extreme emission angles should be greatly influenced by topography. Not to mention the fact that Titan is rather smooth, topographically speaking, with only a couple km elevation variation on the surface ([Corlies et al. 2017](#)).

Despite this clear deviation at high emission, the model and data still match remarkably well. Nowhere is this easier shown than the azimuth skewers, which unlike the incidence and emission skewers, regularly have data in large numbers and data points covering the entire range. And in most situations, the result is flat, such as in [Figure 16](#) and [Figure 17](#).

[Figure 16](#) importantly demonstrates in its short wavelength windows that we can still have points below 0.0 albedo even at low emission angles, not just high ones; indicating that there are probably at least two effects influencing this result. However, dark as the data are, they are all flat and

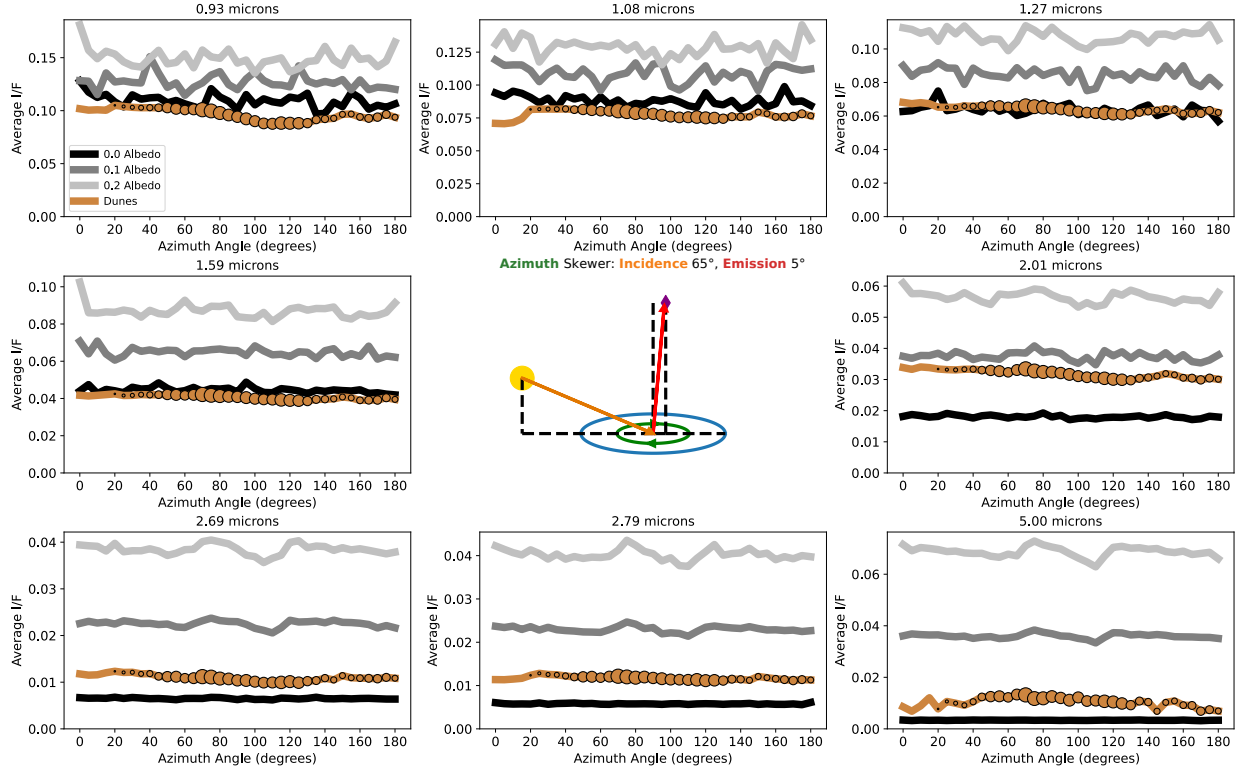


**Figure 16.** Same as Figure 11 but is instead a skewer through the azimuth angle, with incidence and emission held fixed.

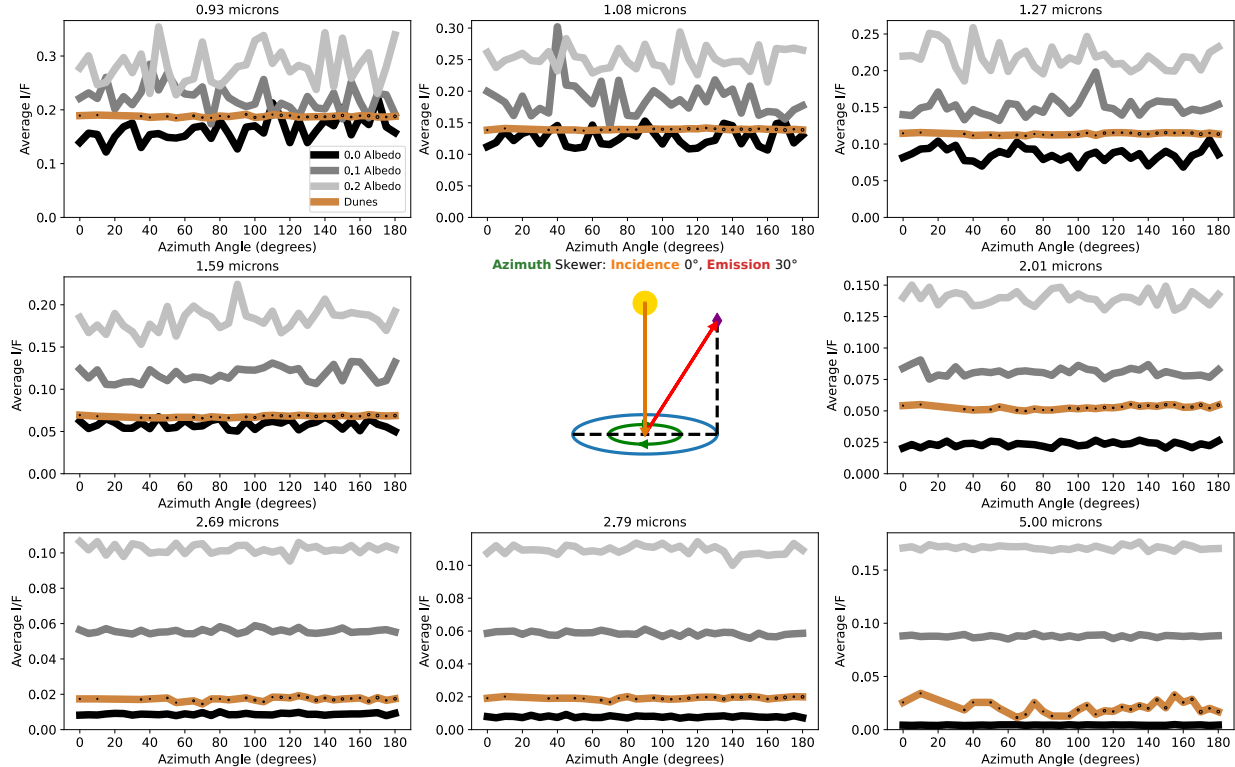


**Figure 17.** Same as [Figure 16](#) but at different fixed incidence and emission angles.

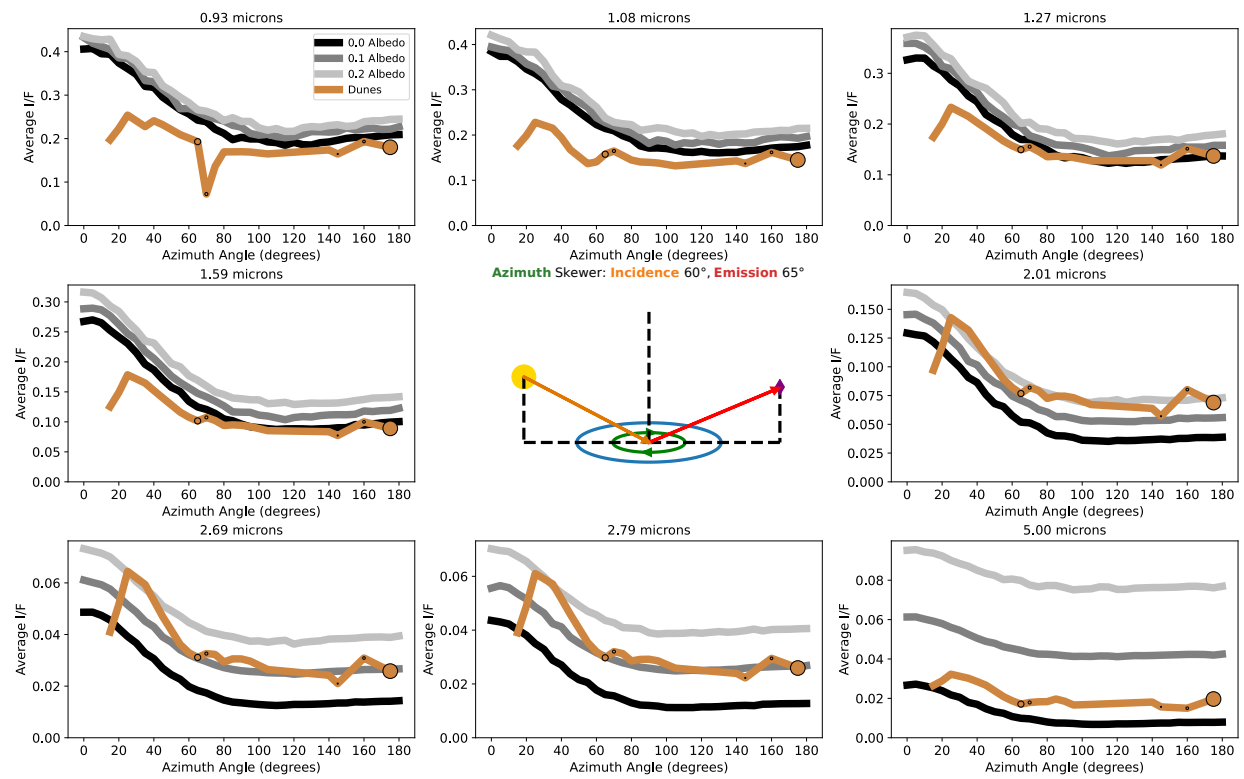


**Figure 18.** Same as [Figure 16](#) but at different fixed incidence and emission angles.

uniform, as the models indicate it should be. Most azimuth views are completely flat in both model and real data.

The exception to the flatness is when both incidence and emission are high at the same time, at which point the models predict low azimuth should be brighter than the other azimuths, as can be seen in [Figure 18](#). Unfortunately, we have very few observations in this region of the phase function, and the interpolation is rather suspect as there aren't other regions with similar behavior as was the case with the emission skewers. [Figure 18](#)'s interpolation still shows an uptick at low azimuth despite this, which at least suggests the behavior is plausibly accurate. One saving grace is that at such angles, the effects of the atmosphere take over and almost drown out the surface effects, so the dunes themselves are unlikely to have much effect on real observations in the first place. Note that in [Figure 18](#) the different albedo values are all very closely clustered together and nearly identical in shape, corroborating this thought. Even though the  $5\ \mu\text{m}$  window seems to be spread out over albedo, this is merely due to the fact that all the models report very dim I/F values, differing only by 0.05 overall.

In the end, where does this leave us? With the shapes of the dunes data matching the phase function models so closely in incidence and azimuth, it seems reasonable to conclude that Titan acts as a lambertian surface. The primary evidence for nonlambertian behavior comes from the emission skewers, which does not appear to have an azimuthal dependence and is likely an atmospheric effect not accounted for in the model, rather than a true non-lambertian phase function. The other minor deviation in [Figure 12](#) correlates directly with the windows brightening in emission skewers, tying the effects together, lowering our expectations of a non-lambertian effect even further.

However, we recognize that our method of binning pixels together and averaging them all makes us significantly less sensitive to dramatic changes over tiny angular extents, such as the sharp central peak seen in the opposition effect, sometimes less than one degree away from opposition ([Kulyk 2008; Schaefer et al. 2008](#)). It is worthwhile to perform a more focused check for such an effect.

### 5.3. Opposition Effect Search

We actively looked for opposition effects in the dune data discussed above and found none—these would occur at places where incidence and emission were close to each other, and azimuth was at or near  $180^\circ$ . We unfortunately had very little data exactly at these points, but if the opposition effect was somewhat broad on Titan, we would have expected to still see some "humps" in the data that would not have been replicated in the models. This was not the case. Forward scattering is not a component of the opposition effect, though it would

be similarly placed in the phase functions, just at  $0^\circ$  azimuth instead. We also do not observe it in our skewers.

However, we would not have noticed an extremely sharp opposition effect, as it could conceivably only matter at angles extremely close to direct opposition; that is, near  $0^\circ$  incidence,  $0^\circ$  emission,  $180^\circ$  azimuth. Our dunes data only has a handful of points around this region, and it is at the very border of the phase function models, so looking at skewers is rather unhelpful. Instead, we went back to the original VIMS cub files and looked for ones of the dunes that had viewing geometries within  $1^\circ$  of opposition. There was precisely one cube in our data set that met this criteria: cub 1574127168 from flyby T37. We then took the data from this cube and plotted its I/F versus the sun-to-spacecraft angle, which is a measure of how close each pixel was to opposition. The result is [Figure 19](#).

While there does appear to be a spike in [Figure 19](#), it happens at around  $3^\circ$  and vanishes as we approach actual opposition. We can identify this feature with a slightly brighter section of the dunes in the lower left of the cube, near the central non-dune strip. We must consider the possibility that this could be a pointing error; Cassini is known to be off by a degree at times ([Barnes et al. 2008](#)). Due to the stretching of the cube, the brighter section is within one geographical degree of the pixels labeled closest to opposition. We examined other VIMS views of the nearby geography from different flybys and found that the dunes consistently get slightly brighter in that direction, regardless of viewing geometry, so this is most likely a persistent feature and not a very narrow opposition effect. **Do we need to make yet another figure for this? Ta, T10, T35 have the observations needed if we do.**

We must contend with the fact that the opposition effect is all but removed by diffuse lighting and indirect viewing angles from scattering ([Schröder & Keller 2008](#)), which certainly occur at the lower wavelength windows. However, this is not true at all windows,  $5.00\ \mu\text{m}$  in particular sees significant unimpeded sunlight even when it is near sunset ([Barnes et al. 2018](#)). If there were an opposition effect being hidden by the atmosphere, we would be able to see it in  $5.00\ \mu\text{m}$ , but we do not. [Figure 19](#)'s  $5.00\ \mu\text{m}$  window in fact has the least evidence of a spike out of all windows.

With the spike explained, we find the increase in brightness with proximity to opposition appears vaguely linear, which is expected ([Kulyk 2008](#)). With this we conclude our search, declaring that we observe no opposition effect whatsoever in the dunes. However, we cannot say for certain that there is no opposition effect—this is a single observation and we have no way of knowing if VIMS pointing was in error. The closest point to true opposition is reported as  $0.25^\circ$  degrees away; assuming this is correct, even it does not entirely rule out a

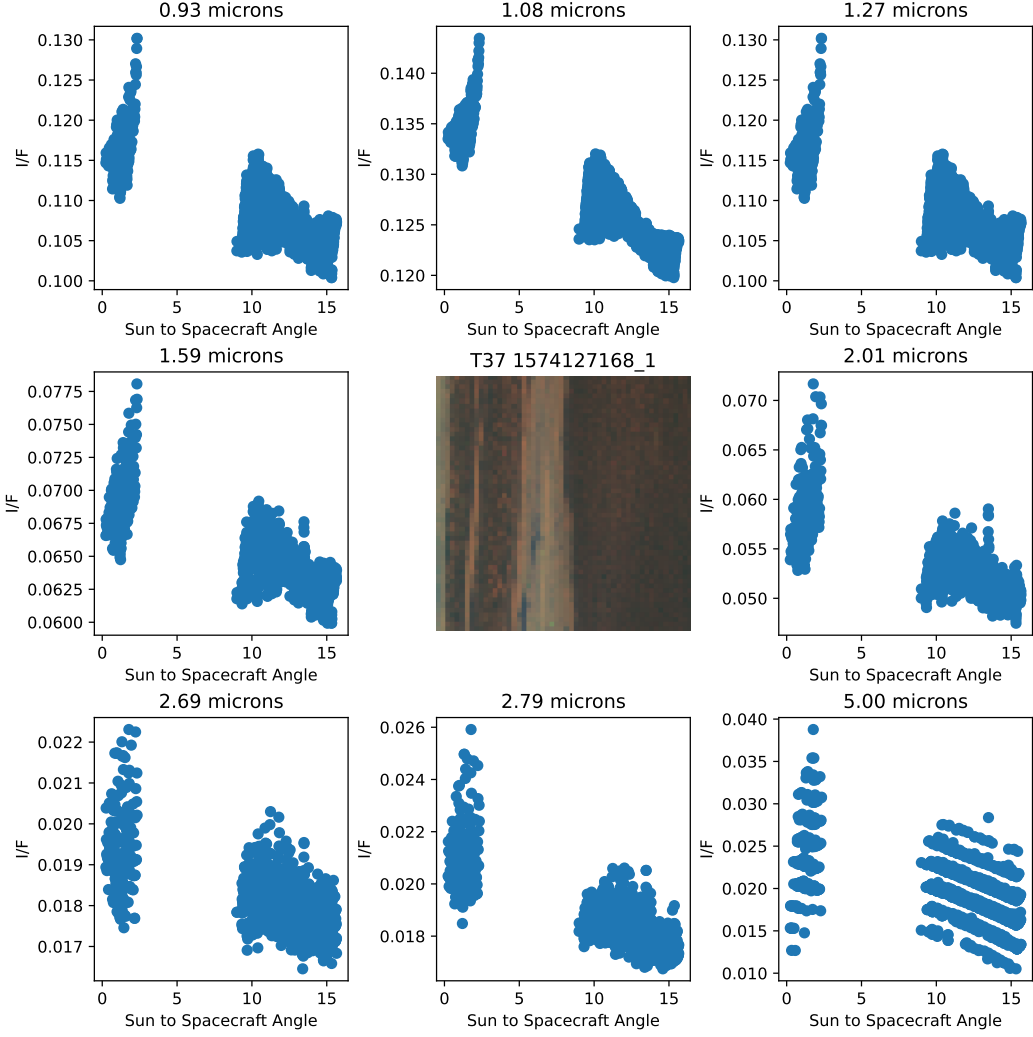


**Figure 19.** NOT FINAL cub 1574127168 from flyby T37 with dunes pixels separated out and plotted by opposition proximity and I/F in all eight windows. The cub itself is plotted in the center with a color scheme of red  $5.00\ \mu\text{m}$ , green  $2.01\ \mu\text{m}$ , and blue  $1.27\ \mu\text{m}$ . Note that the image is significantly stretched, the actual surface of Titan covered by this image is significant, and greatly extended in the horizontal direction. The gap in the middle of the points exists due to those pixels not being dune pixels. Note that most of the points follow a generally linear trend with the exception of a single spike at around  $3^\circ$  from opposition. We can visually see some somewhat brighter dunes pixels in the central image in the lower left, which no doubt cause this spike. The physical location of the pixels closest to true opposition are in the upper left region.

narrow and sharp opposition effect, as these can be confined to within  $0.1^\circ$  (Kulyk 2008; Schaefer et al. 2008).

## 6. SUMMARY AND CONCLUSION

There were two primary purposes to this paper: to validate the SRTC++ simulation against real data, and to identify how Lambertian Titan's dunes were.

On the validation front, SRTC++ in general gave phase function trends that matched the real data, but is clearly not always getting the correct albedo, as evidenced by situations where the recovered albedo is below 0.0, an impossibility. As these moments primarily occur at short wavelengths, this could be the influence of Rayleigh Scattering. Alternatively, or perhaps additionally, its source could be a mistake in the

atmospheric characterization—the deviations along emission skewers imply there's certainly something missing there.

Despite these caveats, SRTC++ still produces smooth lines that stand alongside the real data in most incidence and azimuthal skewers, only with inconsistent albedo results. As such, the simulations are still useful for characterizing Titan's surface, particularly looking for clear deviations from the Lambertian ideal. It is telling, then, that we found almost none. There is no evidence of an opposition effect and no evidence of a forward scattering component. The only potential deviation is the curious dimming and brightening some windows exhibit at high emission angles—but as this effect is azimuthally agnostic, it is most likely an atmospheric effect the model doesn't account for, not a surface effect.

617 Which leaves us with a profound result: Titan's dunes are  
 618 lambertian surfaces, or very close to it. This is opposed to  
 619 the other icy Saturnian moons which have clear opposition  
 620 effects (Kulyk 2008). What makes Titan this way? While it  
 621 is not the focus of this paper to come up with physical expla-  
 622 nations, we can speculate that, since Titan is theorized to be  
 623 covered in organic tholins, they may cover the ice and hide  
 624 its optical properties from incoming light. We note that radar  
 625 observations do, in fact, observe an opposition effect in the  
 626 dunes despite how generally dark they are in such measure-  
 627 ments (Neish et al. 2010; Wye 2011). This disagreement is  
 628 not unusual, as the length scales over which radar and VIMS  
 629 probe are vastly different.

630 To be fair, Earth sand is also generally lambertian (Hapke  
 631 & van Hoen 1963), though unlike Titan, Earth's dune terrains  
 632 are quite bright. However, even sand on Earth exhibits the  
 633 opposition effect within two degrees of ideal (Wise & Mars  
 634 2022), so the fact that we don't see any sign of it is curious.

635 Future work on this front would include improving  
 636 SRTC++ to emulate the atmosphere properly at high

637 emission—or, if that were to prove impossible, investigating  
 638 what other effects might cause the inaccuracies at high emis-  
 639 sion. This work could also be turned to the specular lakes at  
 640 Titan's north pole; while the atmosphere is not as well char-  
 641 acterized there, we can use the relatively simple lake phase  
 642 functions to probe where specifically it's poorly character-  
 643 ized. Other terrain types on Titan could also be examined—it  
 644 would just require a manual rather than automated approach,  
 645 as the other terrains are not as distinct as the dunes. Prelimi-  
 646 nary investigations on this front can be found in the appendix.

647 Acknowledgements:

648 **Data availability?** Would like to make it clear that we'll  
 649 give all the information after just being asked... and help-  
 650 ful reviewers as well, but that comes later.

651 **[Not sure who needs to be put here who won't be put  
 652 on the author list. Though there is going to be funding  
 653 recognition here.]**

654

## APPENDIX

655

### A. EQUATORIAL BRIGHT TERRAIN

656 Like the dunes, the equatorial bright terrain (known as "plains" in radar maps) is extensive and has lots of observations over  
 657 many viewing geometries. Originally we had planned to treat it alongside the dunes and use both to bolster our conclusions.  
 658 However, as can be seen in [Figure 20](#), the equatorial bright terrain was far less well-behaved than the dunes.

659 If the inconsistency in the equatorial bright terrain was predictable, then we would likely have continued to try to draw con-  
 660 clusions from it. However, as we can see in [Figure 20](#), the observations have large stretches where the points are in line, before  
 661 suddenly jumping up or down. This forces us to conclude that what is labeled as equatorial bright terrain is actually multiple  
 662 different terrain types with their own phase functions. This is not just a distinction between flat areas and mountains—while VIMS  
 663 has a hard time differentiating those, the radar data used to make the terrain maps had a separate "hummocky" terrain type that  
 664 was not included in the equatorial bright terrain mask.

665 In general, the equatorial bright terrain would follow the lines of the phase function models, and it too exhibits the deviations  
 666 at high emission. But any other deviations we noted could not have anything else said about them, and even the level to which  
 667 the terrain followed the models' shapes was suspect. A dedicated investigation will likely need to be devoted to this terrain in the  
 668 future, perhaps even extending it beyond the equatorial regions if that is deemed reasonable.

## REFERENCES

- 669 Barnes, J. W., MacKenzie, S. M., Lorenz, R. D., & Turtle, E. P.  
 670 2018, The Astronomical Journal, 156, 247,  
 671 doi: [10.3847/1538-3881/aae519](https://doi.org/10.3847/1538-3881/aae519)
- 672 Barnes, J. W., Brown, R. H., Turtle, E. P., et al. 2005, Science, 310,  
 673 92, doi: [10.1126/science.1117075](https://doi.org/10.1126/science.1117075)
- 674 Barnes, J. W., Brown, R. H., Soderblom, L., et al. 2007, Icarus,  
 675 186, 242, doi: [10.1016/j.icarus.2006.08.0219](https://doi.org/10.1016/j.icarus.2006.08.0219)
- 676 —. 2008, Icarus, 195, 400, doi: [10.1016/j.icarus.2007.12.006](https://doi.org/10.1016/j.icarus.2007.12.006)
- 677 Brossier, J. F., Rodriguez, S., Cornet, T., et al. 2018, Journal of  
 678 Geophysical Research: Planets, 123, 1089–1112,  
 679 doi: [10.1029/2017je005399](https://doi.org/10.1029/2017je005399)
- 680 Buratti, B., Sotin, C., Brown, R., et al. 2006, Planetary and Space  
 681 Science, 54, 1498, doi: [10.1016/j.pss.2006.06.015](https://doi.org/10.1016/j.pss.2006.06.015)
- 682 Cooper, C. A., Robinson, T. D., Barnes, J. W., Mayorga, L. C., &  
 683 Robinthal, L. 2025, Extreme Forward Scattering Observed in  
 684 Disk-Averaged Near-Infrared Phase Curves of Titan, arXiv,  
 685 doi: [10.48550/ARXIV.2507.00924](https://doi.org/10.48550/ARXIV.2507.00924)

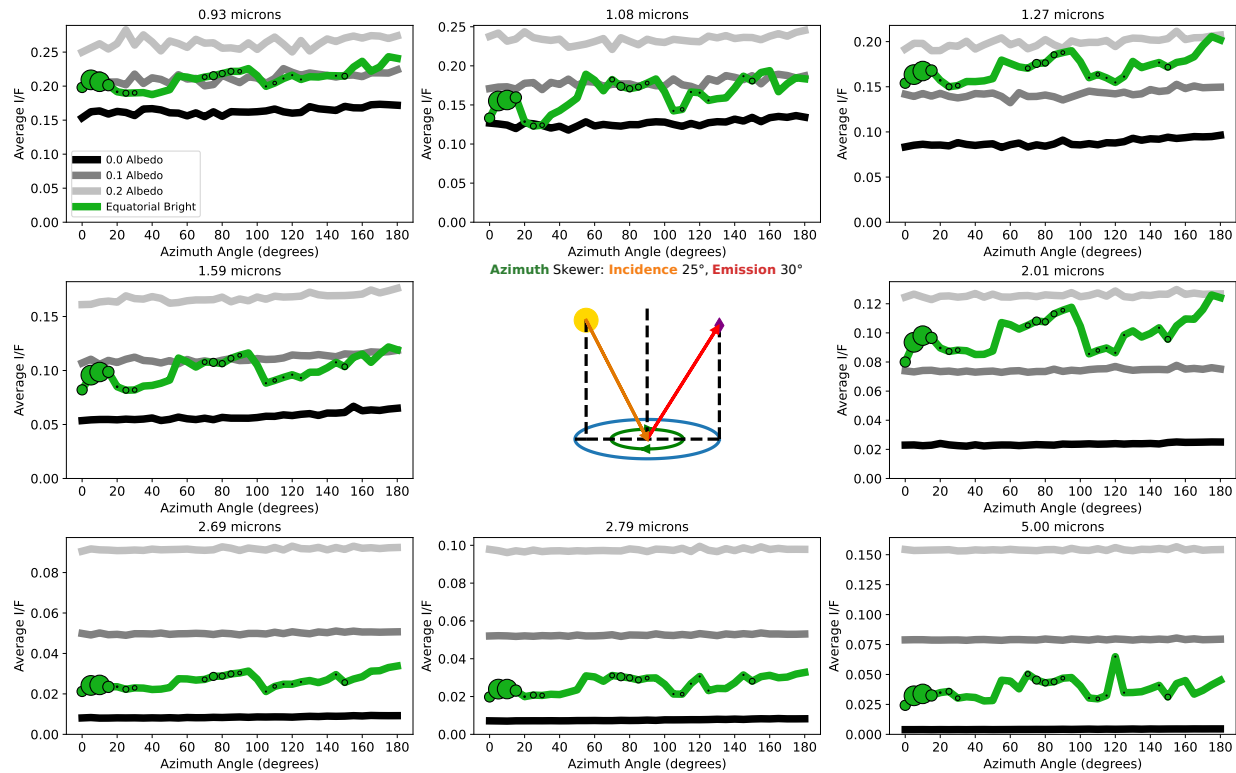


**Figure 20.** Azimuth angle skewer: azimuth angle versus average I/F comparing phase function models with equatorial bright data with fixed incidence and emission angles. Showcases all eight wavelengths arranged from shortest to longest, with the central area occupied by a geometry diagram to illustrate the exact situation plotted. Model lines are monochromatic, equatorial bright data are green. Places with direct equatorial bright observations have dots plotted overtop of the lines, larger dots meaning more observations. Places on the equatorial bright lines without dots are interpolated values. Note that the vertical axis scales with the data, not all wavelengths produce the same average I/F scale.

- 686 Corlies, P., Hayes, A. G., Birch, S. P. D., et al. 2017, Geophysical  
687 Research Letters, 44, doi: [10.1002/2017gl075518](https://doi.org/10.1002/2017gl075518)
- 688 Corlies, P., McDonald, G. D., Hayes, A. G., et al. 2021, Icarus,  
689 357, 114228, doi: [10.1016/j.icarus.2020.114228](https://doi.org/10.1016/j.icarus.2020.114228)
- 690 Déau, E., Dones, L., Rodriguez, S., Charnoz, S., & Brahic, A.  
691 2009, Planetary and Space Science, 57, 1282,  
692 doi: [10.1016/j.pss.2009.05.005](https://doi.org/10.1016/j.pss.2009.05.005)
- 693 Es-sayeh, M., Rodriguez, S., Coutelier, M., et al. 2023, The  
694 Planetary Science Journal, 4, 44, doi: [10.3847/PSJ/acbd37](https://doi.org/10.3847/PSJ/acbd37)
- 695 García Muñoz, A., Lavvas, P., & West, R. A. 2017, Nature  
696 Astronomy, 1, doi: [10.1038/s41550-017-0114](https://doi.org/10.1038/s41550-017-0114)
- 697 Griffith, C. A., Doose, L., Tomasko, M. G., Penteado, P. F., & See,  
698 C. 2012, Icarus, 218, 975, doi: [10.1016/j.icarus.2011.11.034](https://doi.org/10.1016/j.icarus.2011.11.034)
- 699 Hapke, B., & van Hoen, H. 1963, Journal of Geophysical  
700 Research, 68, 4545–4570, doi: [10.1029/jz068i015p04545](https://doi.org/10.1029/jz068i015p04545)
- 701 Hayes, A. G. 2016, Annual Review of Earth and Planetary  
702 Sciences, 44, 57, doi: [10.1146/annurev-earth-060115-012247](https://doi.org/10.1146/annurev-earth-060115-012247)
- 703 Kazeminejad, B., Atkinson, D. H., & Lebreton, J.-P. 2011, The  
704 Astrophysical Journal Letters, 47, 1622–1632,  
705 doi: [10.1016/j.asr.2011.01.019](https://doi.org/10.1016/j.asr.2011.01.019)
- 706 Kulyk, I. 2008, Planetary and Space Science, 56, 386–397,  
707 doi: [10.1016/j.pss.2007.11.011](https://doi.org/10.1016/j.pss.2007.11.011)
- 708 Lopes, R. M. C., Malaska, M. J., Schoenfeld, A. M., et al. 2020,  
709 Nature Astronomy, 4, 228, doi: [10.1038/s41550-019-0917-6](https://doi.org/10.1038/s41550-019-0917-6)
- 710 Lynch, D. K., & Livingston, W. 2004, Color and light in nature  
711 (Cambridge Univ. Press)
- 712 Neish, C. D., Lorenz, R. D., Kirk, R. L., & Wye, L. C. 2010,  
713 Icarus, 208, 385–394, doi: [10.1016/j.icarus.2010.01.023](https://doi.org/10.1016/j.icarus.2010.01.023)
- 714 Pont, S. C., & Koenderink, J. J. 2007, Perception amp;  
715 Psychophysics, 69, 459–468, doi: [10.3758/bf03193766](https://doi.org/10.3758/bf03193766)
- 716 Rannou, P., Coutelier, M., Rivière, E., et al. 2021, The  
717 Astrophysical Journal, 922, 239,  
718 doi: [10.3847/1538-4357/ac2904](https://doi.org/10.3847/1538-4357/ac2904)
- 719 Schaefer, B. E., Rabinowitz, D. L., & Tourtellotte, S. W. 2008, The  
720 Astronomical Journal, 137, 129–144,  
721 doi: [10.1088/0004-6256/137/1/129](https://doi.org/10.1088/0004-6256/137/1/129)
- 722 Schröder, S., & Keller, H. 2008, Planetary and Space Science, 56,  
723 753–769, doi: [10.1016/j.pss.2007.10.011](https://doi.org/10.1016/j.pss.2007.10.011)
- 724 Seal, D., & Bittner, M. 2017, in 2017 IEEE Aerospace Conference  
725 (IEEE), 1–12, doi: [10.1109/aero.2017.7943848](https://doi.org/10.1109/aero.2017.7943848)
- 726 Soderblom, L. A., Kirk, R. L., Lunine, J. I., et al. 2007, Planetary  
727 and Space Science, 55, 2025, doi: [10.1016/j.pss.2007.04.014](https://doi.org/10.1016/j.pss.2007.04.014)
- 728 Soderblom, L. A., Brown, R. H., Soderblom, J. M., et al. 2009,  
729 Icarus, 204, 610, doi: [10.1016/j.icarus.2009.07.033](https://doi.org/10.1016/j.icarus.2009.07.033)

- 730 Solomonidou, A., Malaska, M., Lopes, R., et al. 2024, Icarus, 421,  
731 116215, doi: [10.1016/j.icarus.2024.116215](https://doi.org/10.1016/j.icarus.2024.116215)
- 732 Sullivan, C. B., & Kaszynski, A. A. 2019, Journal of Open Source  
733 Software, 4, 1450, doi: [10.21105/joss.01450](https://doi.org/10.21105/joss.01450)
- 734 Tomasko, M. G., Doose, L., Engel, S., et al. 2008, Planetary and  
735 Space Science, 56, 669, doi: [10.1016/j.pss.2007.11.019](https://doi.org/10.1016/j.pss.2007.11.019)
- 736 Wise, J. E., & Mars, J. C. 2022, Remote Sensing, 14, 5020,  
737 doi: [10.3390/rs14195020](https://doi.org/10.3390/rs14195020)
- 738 Wye, L. C. 2011, Radar scattering from Titan and Saturn's icy  
739 satellites using the Cassini spacecraft (stanford university)
- 740 Xu, F., West, R. A., & Davis, A. B. 2013, Journal of Quantitative  
741 Spectroscopy and Radiative Transfer, 117, 59,  
742 doi: [10.1016/j.jqsrt.2012.10.013](https://doi.org/10.1016/j.jqsrt.2012.10.013)